compound **10** has a reasonably large δ value, and its fluorescence quantum yield is low in comparison with **3**, consistent with efficient intersystem crossing. Preliminary results indicate that **10** is a singlet O_2 sensitizer, which makes it a good candidate for cytotoxicity and photodynamic therapy studies in biological tissues (*16*).

We suggest that π-conjugated molecules with large changes of quadrupole moment upon excitation are worthy of examination as molecules with large two-photon absorption cross sections. Molecules derived from the design strategies described should greatly facilitate a variety of applications of two-photon excitation in biology, medicine, three-dimensional optical memory, photonics, (*17*) optical limiting (*2*), and materials science (*17*).

References and Notes

1. W. Denk, J. H. Strickler, W. W. Webb, *Science* **248**, 73 (1990); R. M. William, D. W. Piston, W. W. Webb, *FASEB J.* **8**, 804 (1994); W. Denk and K. Svoboda, *Neuron* **18**, 351 (1997); R. H. Köhler, J. Cao, W. R. Zipfel, W. W. Webb, M. R. Hansen, *Science* **276**, 2039 (1997).
2. J. E. Ehrlich *et al.*, *Opt. Lett.* **22**, 1843 (1997).
3. A. A. Said *et al.*, *Chem. Phys. Lett.* **228**, 646 (1994); G. S. He, R. Gvishi, P. N. Prasad, B. Reinhardt, *Opt. Commun.* **117**, 133 (1995).
4. D. A. Parthenopoulos and P. M. Rentzepis, *Science* **245**, 843 (1989); J. H. Strickler and W. W. Webb, *Opt. Lett.* **16**, 1780 (1991).
5. W. Denk, *Proc. Natl. Acad. Sci. U.S.A.* **91**, 6629 (1997).
6. R. R. Birge, *Acc. Chem. Res.* **19**, 138 (1986).
7. C. Xu and W. W. Webb, *J. Opt. Soc. Am. B* **13**, 481 (1996); C. Xu *et al.*, *Proc. Natl. Acad. Sci. U.S.A.* **93**, 10763 (1996).
8. R. J. M. Anderson, G. R. Holtom, W. M. McClain, *J. Chem. Phys.* **70**, 4310 (1979).
9. M. J. S. Dewar, E. G. Zoebisch, E. F. Healy, J. J. P. Stewart, *J. Am. Chem. Soc.* **107**, 3902 (1985).
10. J. Ridley and M. Zerner, *Theoret. Chim. Acta* **32**, 111 (1973).
11. R. J. Buenker and S. D. Peyerimhoff, *ibid.* **35**, 33 (1974).
12. B. Dick, R. M. Hochstrasser, H. P. Trommsdorff, in *Nonlinear Optical Properties of Organic Molecules and Crystals*, D. S. Chemla and J. Zyss, Eds. (Academic Press, Orlando, FL, 1987), vol. 2, pp. 167–170.
13. B. J. Orr and J. F. Ward, *Mol. Phys.* **20**, 513 (1971).
14. The two-photon absorption cross sections were determined by two-photon–excited fluorescence measurements, with 5-ns, 10-Hz pulses from a Nd:yttrium-aluminum-garnet–pumped optical parametric oscillator-amplifier system. The setup consisted of two arms to allow relative measurements with respect to bis-1,4-(2-methylstyryl)benzene (in cyclohexane), fluorescein (in pH 11 water), and rhodamine B (in methanol). The sample chromophores were dissolved in toluene (10^{-4} M concentration); an approximately collimated beam was used to excite the samples over the 1-cm length of the cuvettes. The fluorescence emitted at right angles to the excitation was collected and focused onto photomultiplier tube detectors. The intensity of the incident beam was adjusted to assure excitation in the intensity-squared regime.
15. S. M. Kennedy and F. E. Lytle, *Anal. Chem.* **58**, 2643 (1986). We scaled the peak δ value reported in this paper by a factor chosen to match the long-wavelength data reported therein with that of (*7*).
16. M. Lipson, M. Levin, S. R. Marder, J. W. Perry, unpublished results.
17. B. H. Cumpston *et al.*, in preparation.

18. Support from the NSF (Chemistry Division), Office of Naval Research, and the Air Force Office of Scientific Research (AFOSR) and its Defense University Research Instrumentation Program at the California Institute of Technology is gratefully acknowledged. The research described in this paper was performed in part by the Jet Propulsion Laboratory, California Institute of Technology, as part of its Center for Space Microelectronics Technology, and was supported by the Ballistic Missile Defense Organization, Innovative Science and Technology Office and AFOSR through an agreement with NASA. The work in Mons was carried out within the framework of the Belgium Prime Minister Office of Science Policy "Pôle d'Attraction Interuniversitaire en Chimie Supramoléculaire et Catalyse" PAI 4/11 and is partly supported by the Belgium National Fund for Scientific Research (FNRS-FRFC) and an IBM-Belgium Academic Joint Study; D.B. is a Chercheur Qualifié FNRS, and T.K. is a Ph.D. grant holder of Fund for Research in Industry and Agriculture. The femtosecond two-photon fluorescence excitation cross-section measurements were carried out in the Developmental Resource for Biophysical Imaging Opto-electronics at Cornell University with support of NIH–National Center of Research Resources and NSF. G.S. acknowledges support from the NASA-JOVE program.

7 May 1998; accepted 31 July 1998

Detection and Modeling of NonTidal Oceanic Effects on Earth's Rotation Rate

Steven L. Marcus, Yi Chao, Jean O. Dickey, Pascal Gegout

Subdecadal changes in Earth's rotation rate, and hence in the length of day (LOD), are largely controlled by variations in atmospheric angular momentum. Results from two oceanic general circulation models (OGCMs), forced by observed wind stress and heat flux for the years 1992 through 1994, show that ocean current and mass distribution changes also induce detectable LOD variations. The close similarity of axial oceanic angular momentum (OAM) results from two independent OGCMs, and their coherence with LOD, demonstrate that global ocean models can successfully capture the large-scale circulation changes that drive OAM variability on seasonal and shorter time scales.

Changes in the rotation rate of the solid Earth (that is, its crust and mantle), typically yield variations in the LOD of about 1 ms over several years (*1*). Earth as a whole conserves its angular momentum (with the exception of tidal torques); LOD variations, in particular, arise largely from compensating changes in atmospheric angular momentum (AAM) carried by zonal (west-to-east) winds (*2, 3*). Remaining discrepancies in the axial budget indicate that other reservoirs also store and release appreciable quantities of angular momentum on these time scales, but these have been less well resolved.

In this study we show that (i) a significant nontidal oceanic signal can be detected in geodetic LOD series and (ii) this contribution of OAM helps to close the global budget on seasonal and shorter time scales. Because the three-dimensional observational data needed to compute OAM directly are not available, we use two OGCM simulations as a proxy for our analysis. These comparisons can provide a valuable check on the realism of the model-derived OAM and may be used to estimate contributions from other angular momentum reservoirs, such as changes in terrestrial and atmospheric water storage.

We consider results from two OGCMs whose dynamical formulations differ considerably: the Modular Ocean Model (*4*) (MOM), based on earlier multilevel models developed at the Geophysical Fluid Dynamics Laboratory (*5*), and a multilayer model based on an early version of the Miami Isopycnal Coordinate Ocean Model (MICOM) (*6*). Both MOM and MICOM are based on the primitive equations of fluid flow that use the Boussinesq and hydrostatic approximations. The major differences between the two models are (i) their vertical coordinate systems: MOM uses geometrical depth beneath a rigid lid and MICOM uses a density-based coordinate with a freely varying surface height; and (ii) their treatment of the surface mixed layer: MOM uses a Richardson-number scheme (*7*) and MICOM uses the Kraus-Turner mixed layer model (*8*). Both models have a horizontal resolution of 2° longitude by 1° latitude and comparable vertical resolution (22 and 12 layers, respectively).

The OGCMs were spun up for 10 years starting from climatological temperature and salinity distributions (*9*), forced with climatological monthly wind stress (*10*) and sea surface temperature and salinity (*9*). The models were then driven with surface wind stress derived from the daily National Center for Environmental Prediction (NCEP) 1000-hPa analysis from 1 January 1992 to 15 December 1994, and heat flux as computed using the bulk formulation described in (*11*);

Jet Propulsion Laboratory, California Institute of Technology, 4800 Oak Grove Drive, Pasadena, CA 91109 USA.

the first 45 days were excluded from the analysis to eliminate transient effects. Pressure forcing by the atmosphere was not included. A shorter experiment (24 September 1992 to 14 March 1994) was also done with the MOM model using surface wind stress derived from the ERS-1 scatterometer (*12*).

The contributions to OAM variation calculated from the zonal currents simulated by each model represent changes in the relative axial angular momentum of the oceans and are expressed in units of equivalent LOD (Fig. 1A). Both models are characterized by a net west-to-east flow, which sequesters positive angular momentum, giving rise to a mean positive LOD forcing of about 100 μs; for comparison the atmosphere has a mean zonal velocity of about 7 ms^{-1} and would change the average LOD by about 2.5 ms were its superrotation to cease (Fig. 2A). Both current terms are characterized by drifts that are approximately linear in time but opposite in sign. Removal of these trends, which reflect the incomplete equilibration of the OGCMs during spinup, leaves relative OAM variations that are similar between the MICOM and MOM simulations; the root mean square (rms) magnitudes are 12.7 and 14.5 μs, respectively.

Because of the background planetary rotation, changes in the oceans' moment of inertia also induce OAM variations (their effect on the relative angular momentum is orders of magnitude smaller and is neglected). Changes in the planetary terms for the two models (Fig. 1B, solid lines) again show long-term trends of opposite sign, although these are not linear and are much larger than the corresponding trends for the relative OAM. Because of the use of the Boussinesq approximation in the governing equations, both models conserve volume rather than mass. The OAM variations due to changes in the total mass content of each model (*13*) are shown by the dashed lines in Fig. 1B and clearly account for the bulk of the long-term trends. Removal of the effects of mass nonconservation, as well as residual linear trends representing incomplete equilibration during spinup, yields time series of planetary OAM that are similar between the MOM and MICOM results; their respective rms magnitudes are 21.2 and 22.5 μs, nearly twice that of the relative OAM.

The total OAM variations obtained by adding the detrended relative and planetary OAM series bear a strong resemblance over the nearly 3 years simulated by the two models with NCEP forcing (Fig. 1C) despite their distinct dynamical formulations and the differences in long-term trends after spinup. The shorter OAM series derived from the MOM model forced by ERS-1 winds resembles the NCEP-forced results over the period of overlap, although its rms magnitude is only 64% as great because of the lower variability of the ERS scatterometer winds (*12*). Thus, simulations of the circulation features that contribute to the axial OAM—that is, the large-scale current systems and mass distribution (*14*)—appear to be robust.

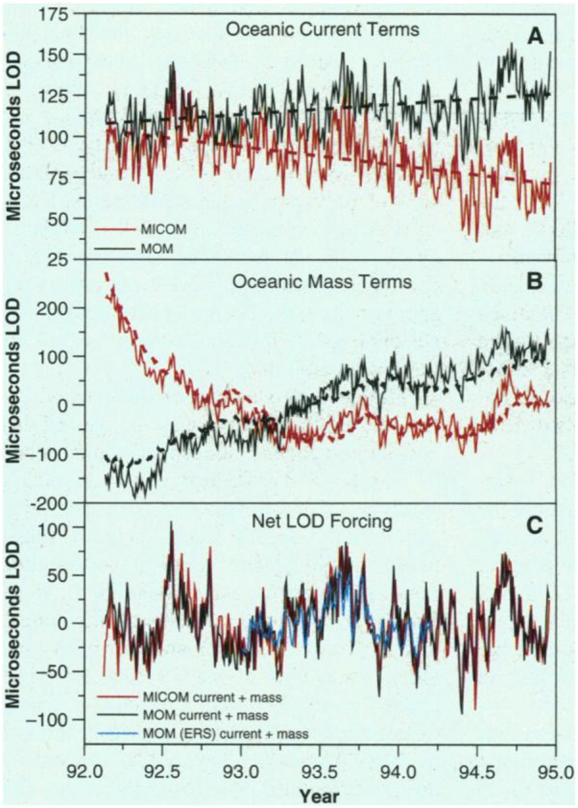

Fig. 1. LOD excitation computed from the OGCM results. Both models were forced with surface wind stress and heat flux computed from daily NCEP analyses; pressure forcing by the atmosphere was not considered. (**A**) Relative OAM contained in zonal currents (solid lines); positive LOD forcing corresponds to a net west-to-east flow. Dashed lines indicate least-squares-fit linear trends for each model series. (**B**) Planetary OAM changes for the two OGCM simulations (solid lines); time mean has been removed from each series. Dashed lines indicate change due to variations in the total mass content of each model (see text for details). (**C**) Sum of relative and planetary OAM changes for each model, after removal of linear trends and the effects of mass nonconservation. The detrended OAM is also shown for a shorter experiment with the MOM model forced by ERS-1 winds.

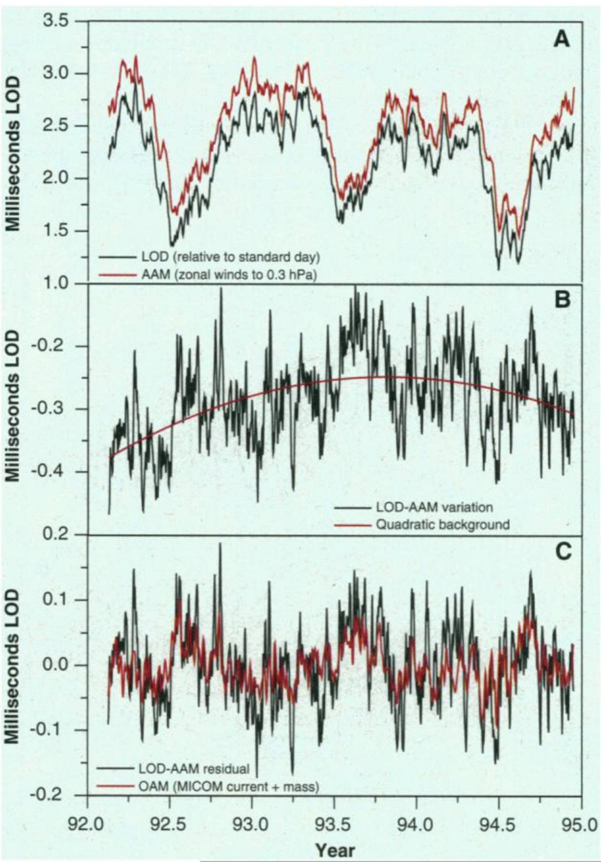

Fig. 2. (**A**) Comparison of observed LOD with atmospheric forcing, computed from zonal winds integrated from 1000 to 0.3 hPa. Because the LOD is defined with respect to an arbitrary reference value, its vertical offset has no physical significance. (**B**) Difference between the LOD and AAM curves plotted in frame (A) compared with a least-squares-fit second-order polynomial used to represent the effects of core-mantle coupling. (**C**) Difference between the LOD-AAM and quadratic terms plotted in frame (B) compared with total OAM computed from the MICOM simulation.

For comparison with an LOD time series, we used the Kalman-filtered SPACE96 calculation (*15*), which is sampled at daily intervals (Fig. 2A). The effects of tidal forcing on both the solid Earth and oceans has been removed from this series (*16*). We also estimated the LOD forcing due to atmospheric winds integrated from 1000 to 0.3 hPa; values below the 10-hPa level were computed as the averages of global wind analyses provided by the European Centre for Medium-Range Weather Forecasts (ECMWF), the Japanese Meteorological Agency (JMA), and the NCEP/National Center for Atmospheric Research (NCAR) reanalysis campaign, whereas those above 10 hPa were obtained from the British Atmospheric Data Centre (BADC) (*17*). Both the geodetic and atmospheric series contain a strong seasonal signal; higher-frequency variability is also clearly shared by the two time series (*18*).

In a closed two-component system consisting of the solid Earth and atmosphere the combined angular momentum would be constant, and this would be reflected by identical (although offset) shapes of the AAM and LOD series (Fig. 2A). Therefore, the nonzero residual variation shown in Fig. 2B (note the difference in vertical scale) implies that an additional angular momentum reservoir is participating in the global budget. Variations in core motions are believed to be responsible for observed decadal-scale excursions of up to several milliseconds in LOD (*1*). As the core is only weakly coupled to the mantle on the shorter time scales considered here (*19*), we accounted for its effect by removing a least-squares-fit quadratic trend from the LOD-AAM variation. The residual LOD-AAM signal (shown in Fig. 2C) represents the missing part of Earth's axial angular momentum budget and has an rms magnitude of 60.5 μs.

The 3-year OAM series generated by the MICOM and MOM models using NCEP forcing (Fig. 1C) have rms magnitudes of 30.7 and 30.5 μs, respectively, and thus potentially represent about half the residual LOD variation. The MICOM series, shown in Fig. 2C with a quadratic background removed, bears a striking similarity to the LOD-AAM residual ($r^2 = 0.77$) and explains 42% of its variance; the MOM series has a correlation coefficient of 0.72 and explains 34% of the variance. The high correlation coefficients from both models (significant at approximately the 3σ level) demonstrate the detection of a nontidal oceanic signal in Earth's rotation rate.

Further understanding of the oceans' effect on Earth rotation may be gained by comparing geodetic, atmospheric, and oceanic signals in the frequency domain. LOD spectra contain strong seasonal peaks, with amplitudes of about 0.3 to 0.4 ms (*20*). These peaks are still evident in our LOD data after removal of the wind excitation in the 1000- to 10-hPa layer (Fig. 3A), although the amplitude has been reduced by an order of magnitude. The winds above 10 hPa (carrying about 1% of the total atmospheric mass) make a disproportionately large contribution to the seasonal AAM cycle (*2*); removal of the excitation attributed to BADC winds (10 to 0.3 hPa) gives a particularly strong reduction in our results at the annual period, where the residual LOD amplitude is now comparable to that of the low-frequency background.

The OAM time series generated by the OGCM runs also contain seasonal rotation signals, as evidenced by the pronounced decrease in the residual LOD amplitudes (Fig. 3A, red lines) at the first two annual harmonics. Removal of the oceanic excitation simulated by both models produces local amplitude minima within a bandwidth of the annual frequency, suggesting that the oceans play a significant role in the axial angular momentum budget on that time scale (*21*). At the semiannual period, both the 10- to 0.3-hPa winds and the oceanic excitation reduce the LOD residual, although the latter has a greater impact. The upper-atmospheric data apparently contain little of the LOD signal at subseasonal periods, because their incorporation into the atmospheric excitation fails to reduce the spectral amplitude relative to the 1000- to 10-hPa residual in that range. The oceanic excitation from both models, by contrast, consistently lowers the LOD residuals at frequencies up to about (25 day)$^{-1}$.

Further evidence for the presence of a rotational signal in the OGCM results can be obtained from their effect on the coherence of LOD with its excitation sources. The atmospheric data sets used in our study produce coherence with LOD significant at the 95% level for all frequencies up to (10 day)$^{-1}$; however, addition of the 10- to 0.3-hPa winds to the 1000- to 10-hPa data yields no consistent improvement at subseasonal frequencies (Fig. 3B, black lines). In contrast, addition of the OAM data from both models to the atmospheric excitation consistently increases the coherence with LOD at frequencies up to (25 day)$^{-1}$ and generally improves the results up to (15 day)$^{-1}$. At higher frequencies, the effects of incorporating the OAM series are mixed. The combined AAM and MICOM excitation gives better overall results, however, and maintains coherence with LOD significant at the 99% level for all frequencies up to (10 day)$^{-1}$.

The superior results obtained with MICOM at high frequency appear to be due to its isopycnal formulation and better treatment of the mixed layer (*22*); in particular, the density-based vertical coordinate allows a more realistic treatment of the effects of bottom topography than the "staircase" representation employed in depth-based models. The future use of in situ and satellite observations in constraining OGCMs and the incorporation of atmospheric pressure forcing will lead to an increasingly accurate picture of oceanic effects on the Earth's rotational dynamics.

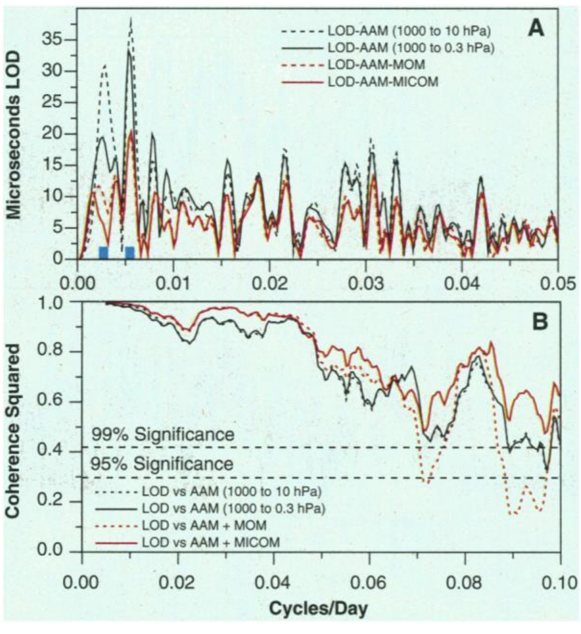

Fig. 3. (**A**) Amplitude spectra of LOD residuals after subtraction of atmospheric and oceanic excitation. AAM was computed from winds supplied by the ECMWF and JMA analysis and NCEP reanalysis campaigns for the 1000- to 10-hPa layer and from BADC winds for the 10- to 0.3-hPa layer; the full (1000 to 0.3 hPa) AAM was used in combination with the OAM computed from the MOM and MICOM results. Spectral bandwidth is given by the width of the blue bars, which are centered on the abscissa at the annual and semiannual frequencies. (**B**) Coherence squared of LOD with atmospheric and combined atmospheric and oceanic excitation sources (note difference in frequency scale).

References and Notes

1. R. Hide and J. O. Dickey, *Science* **253**, 629 (1991); R. D. Rosen, *Surv. Geophys.* **14**, 1 (1993).
2. R. D. Rosen and D. A. Salstein, *Geophys. Res. Lett.* **18**, 1925 (1991).
3. Significant coherence between time series of LOD and AAM extends to periods as short as about 10 days, with loss of coherence at higher frequencies resulting from declining signal-to-noise ratios in both data types [J. O. Dickey, S. L. Marcus, J. A. Steppe, R. Hide, *Science* **255**, 321 (1992)].

4. R. Pacanowski, K. Dixon, A. Rosati, Modular Ocean Model Users' Guide (Geophysical Fluid Dynamics Laboratory, National Oceanic and Atmospheric Administration, Princeton, NJ, 1991).
5. K. Bryan, *J. Comput. Phys.* **4,** 347 (1969); M. D. Cox, *GFDL Ocean Group Tech. Rep. No. 1* (1984).
6. R. Bleck, H. P. Hanson, D. M. Hu, E. B. Kraus, *J. Phys. Oceanogr.* **19,** 1417 (1989); R. Bleck, C. Rooth, D. M. Hu, L. T. Smith, *ibid.* **22,** 1486 (1992); D. M. Hu, *ibid.* **27,** 96 (1997)
7. R. Pacanowski and S. G. H. Philander, *ibid.* **11,** 1443 (1981).
8. E. B. Kraus and J. S. Turner, *Tellus* **19,** 98 (1967).
9. S. Levitus, *Climatological Atlas of the World Ocean* (NOAA Professional Pap. No. 13, Government Printing Office, Washington, DC, 1982).
10. S. Hellerman and M. Rosenstein, *J. Phys. Oceanogr.* **13,** 1093 (1983).
11. Y. Chao and L.-L. Fu, *J. Geophys. Res.* **100,** 24965 (1995).
12. L.-L. Fu and Y. Chao, *Geophys. Res. Lett.* **24,** 1783 (1997).
13. The OAM variation was calculated by assuming the spurious mass change to be distributed uniformly over the oceanic surface layer, following R. J. Greatbatch, *J. Geophys. Res.* **99,** 12767 (1994). The results obtained by assuming the spurious mass change to be distributed uniformly over the oceanic interior are similar.
14. J. C. McWilliams, *Annu. Rev. Fluid Mech.* **28,** 215 (1996); for a general discussion of Earth rotation excitation by geophysical fluids see R. T. H. Barnes, R. Hide, A. A. White, C. A. Wilson, *Proc. R. Soc. London, Ser. A* **387,** 31 (1983). We found that the barotropic component of the MOM model produces OAM variations, which are very similar to the full MOM results, indicating a dominant role for barotropic dynamics in seasonal and shorter OAM variations. The rapid adjustment time of the barotropic modes [R. M. Ponte, *J. Geophys. Res.* **95,** 11369 (1990)] enables the OGCMs to produce realistic OAM variations in spite of the incomplete equilibration of the model fields evident in Fig. 1, A and B.
15. R. S. Gross, in *1996 IERS Annual Report*, M. Feissel, Ed. (Observatoire de Paris, France, 1997), p. 1129.
16. S. D. Desai, thesis, University of Colorado (1996).
17. AAM values were provided by the Sub-Bureau for Atmospheric Angular Momentum of the International Earth Rotation Service [D. A. Salstein, D. M. Kann, A. J. Miller, R. D. Rosen, *Bull. Am. Meteorol. Soc.* **74,** 67 (1993)], based on operational analyses from ECMWF and JMA. Data from the NCEP/NCAR 40-Year Reanalysis Project were used to calculate the NCEP AAM series; see D. A. Salstein and R. D. Rosen, in *7th Conference on Climate Variations* (American Meteorological Society, Boston, MA, 1997), p. 344. AAM values above 10 hPa were computed from gridded wind data taken from the UK Meteorological Office's Assimilated Data for Upper Atmosphere Research Satellite files and provided by the BADC; for details, see R. Swinbank and A. O'Neill, *Mon. Weather Rev.* **122,** 686 (1994).
18. For the atmosphere, variations in axial angular momentum arising from moment-of-inertia changes are about an order of magnitude smaller than those driven by zonal winds (*1*) and involve mass fluctuations due to water vapor. Although these effects are large enough to significantly affect closure of the global budget, their consistent treatment requires full consideration of the hydrological cycle and is beyond the scope of this study.
19. R. Hide, in *Dynamics of Earth's Deep Interior and Earth Rotation*, J.-L. Le Mouel, D. E. Smylie, T. Herring, Eds. (American Geophysical Union, Washington, DC, 1993), pp. 109–112.
20. R. S. Gross, S. L. Marcus, T. M. Eubanks, J. O. Dickey, C. L. Keppenne, *Geophys. Res. Lett.* **23,** 3373 (1996).
21. R. M. Ponte and R. D. Rosen, *J. Phys. Oceanogr.* **24,** 1966 (1994); F. O. Bryan, *Dyn. Atmos. Oceans* **25,** 191 (1997). Both of these studies found sizable annual signals in 1-year samples of OAM taken from OGCM runs forced by monthly mean climatological winds; however, no comparisons using synoptic geodetic or atmospheric data were made.
22. D. Hu and Y. Chao, *Mon. Weather Rev.*, in press.

23. We thank M. Ghil, R. Gross, R. Hide, and two anonymous reviewers for useful comments on the manuscript. We are very grateful to D. Hu, who helped with the MICOM integration, and to D. Dong for the OAM calculation. Computations were performed on the Cray J-90 computer through the JPL Supercomputing project. The work of the authors was carried out by the Jet Propulsion Laboratory, California Institute of Technology, under contract with NASA.

11 May 1998; accepted 28 July 1998

Energetics of Amino Acid Synthesis in Hydrothermal Ecosystems

J. P. Amend* and E. L. Shock

Thermodynamic calculations showed that the autotrophic synthesis of all 20 protein-forming amino acids was energetically favored in hot (100°C), moderately reduced, submarine hydrothermal solutions relative to the synthesis in cold (18°C), oxidized, surface seawater. The net synthesis reactions of 11 amino acids were exergonic in the hydrothermal solution, but all were endergonic in surface seawater. The synthesis of the requisite amino acids of nine thermophilic and hyperthermophilic proteins in a 100°C hydrothermal solution yielded between 600 and 8000 kilojoules per mole of protein, which is energy that is available to drive the intracellular synthesis of enzymes and other biopolymers in hyperthermophiles thriving in these ecosystems.

Recently, Woese (*1*) suggested that the ancestor of all life on Earth was not a discrete entity but rather a community of cells with a shared physical history. Over time, as the universal tree of life radiated outward from the root, three primary domains of organisms arose. Although interpretations of the complete genomes of over a dozen microbes have raised questions regarding the classification of various organisms within this phylogenetic tree (*2*), general properties of members belonging to the deepest branches of the Bacteria and Archaea lineages indicate that the earliest life was autotrophic not heterotrophic, relied on chemosynthesis rather than photosynthesis, and required high temperatures for growth (*3*). On the basis of these findings, ancient hydrothermal systems have been proposed as likely sites for the origin of life (*4–6*). This view is consistent with the results of hydrothermal experiments that were aimed at identifying the primordial chemosynthesis reactions for life's origin (*7*).

In the speculative arena of the origin and the early evolution of life, quantification of the energetics of biosynthesis reactions in microorganisms belonging to the deepest branches in the phylogenetic tree is of interest. However, the determination of these energetics in hydrothermal systems on early Earth (*4, 8, 9*) is hindered somewhat by poorly constrained chemical and physical properties of the earliest oceans, including the redox state, pH, temperature, and concentrations of CO_2, NH_4^+, and H_2S. On the other hand, ample data are available from active hydrothermal ecosystems, which are hosts to the deepest branches of thermophilic, chemoautotrophic Archaea and Bacteria. Analyses of seawater and vent fluids together with reliable equations of state for aqueous organic and inorganic compounds permit well-constrained calculations of the energetics of biosynthesis reactions in hydrothermal ecosystems. Once such a framework for evaluating the energetics of biosynthesis is in place, analogous calculations can be carried out to account for likely conditions on early Earth.

Chemical disequilibria in hydrothermal ecosystems provide substantial amounts of energy, which can drive anabolic reactions in thermophilic and hyperthermophilic chemoautotrophs (*8, 10*). Furthermore, the formation of many aqueous organic compounds is favored at high temperatures over low temperatures (*11–13*). We calculated the overall Gibbs free energies (ΔG_r) of net amino acid synthesis reactions (*r*) for hydrothermal systems and contrasted them with the energy requirements of synthesis reactions in surface seawater. We then used these calculations to explore the ramifications for the synthesis of thermophilic proteins, and we considered the implications for early life.

Amino acid synthesis pathways in extant microorganisms, although highly diverse, share two basic features: (i) the nitrogen of α-amino groups in amino acids originates from NH_4^+ and (ii) the sources of skeletal carbons are intermediates of the tricarboxylic acid cycle and the other major metabolic

Group Exploring Organic Processes in Geochemistry (GEOPIG), Department of Earth and Planetary Sciences, Washington University, St. Louis, MO 63130, USA.

*To whom correspondence should be addressed.